Green Chemistry

PAPER

View Article Online
View Journal | View Issue

Cite this: *Green Chem.*, 2025, **27**, 5051

Tuning the electronic structure of phosphonic acid-based deep eutectic solvents for synergistic catalytic oxidative desulfurization†

Lixian Xu,[a] Jie Yin,[a] Dongao Zhu,[a] Beibei Zhang,[b] Linhua Zhu,[c] Hongping Li,[a] Jing He,[a] Huaming Li[a] and Wei Jiang *[a]

Deep eutectic solvents (DESs) hold immense potential in extraction-coupled oxidative desulfurization; however, their efficient utilization, in terms of catalytic activity and cycle-regeneration stability, remains a significant challenge. Herein, we propose a strategy for constructing bifunctional phosphonic acid-based DESs (PDESs) using zinc chloride ($ZnCl_2$) combined with organic phosphonic acids to achieve ultradeep desulfurization by inducing strong electronic interaction *via* coordination regulation. Through experimental and theoretical screening, the PDES $ZnCl_2$/phenylphosphinic acid ($ZnCl_2$/PIA = 1 : 2), demonstrating strong electron transfer capability and high adsorption energy for oxidants, exhibits remarkable catalytic performance towards the removal of heterocyclic thiophenes. Notably, PDESs can simultaneously function as extractants and catalysts, maintaining a desulfurization efficiency of up to 98.4% even after 12 consecutive cycles under mild conditions, which is much higher than that of previously reported DESs-based desulfurization systems. Furthermore, a possible reaction mechanism is proposed, wherein heterocyclic thiophenes are extracted by the $ZnCl_2$/2PIA PDES *via* strong interactions (*e.g.* hydrogen bonding, C–H···π and π···π) and are then rapidly oxidized by reactive oxygen radicals and peroxy acid in the presence of an oxidant. This study provides a feasible strategy for achieving strong electronic transfer *via* coordination regulation, aimed at developing high-performance DESs for deep desulfurization and other related application.

Received 19th January 2025,
Accepted 28th March 2025

DOI: 10.1039/d5gc00327j

rsc.li/greenchem

Green foundation

1. This study reports the synthesis of a series of multifunctional and adjustable phosphonic acid-based deep eutectic solvents (PDESs) using easily available zinc chloride as the hydrogen bond acceptor for clean fuel production under mild conditions and provides an efficient strategy for tuning the electronic structure *via* coordination regulation.
2. The conversion rate and cycle testing demonstrated the significant environmental benefits of using highly catalytic and stable PDESs as alternatives to organic solvents in extraction-coupled oxidation reactions. After 12 consecutive cycles without any treatment, the desulfurization efficiency of $ZnCl_2$/2PIA remained as high as 98.4%.
3. Future research should focus on optimizing PDES design to achieve properties such as lower viscosity and broader substrate compatibility. Additionally, efforts should be directed toward integrating renewable energy and energy-efficient separation technologies to achieve sustainable reactions and closed-loop recovery, promoting cleaner fuel production.

Introduction

Owing to the rapid development of industry and economy, pollutants like SO_x emitted through the combustion of sulfur compounds from fossil fuels pose great harm to the environment and human health.[1–3] Reducing sulfur content at the source is an effective strategy to meet stricter environmental requirements for clean fuel production. To this end, various benign and scalable desulfurization technologies, including extractive desulfurization (EDS) and oxidative desulfurization (ODS), can be employed owing to their high efficiency for per-

[a]*Institute for Energy Research, Jiangsu University, Zhenjiang 212013, P. R. China. E-mail: jiangwei@ujs.edu.cn*
[b]*College of Chemistry and Chemical Engineering, Yancheng Institute of Technology, Yancheng 224061, P. R. China*
[c]*College of Chemistry and Chemical Engineering, Key Laboratory of Water Pollution Treatment and Resource Reuse of Hainan Province, Hainan Normal University, Haikou 571158, P.R. China*

† Electronic supplementary information (ESI) available. See DOI: https://doi.org/10.1039/d5gc00327j

sistent heterocyclic thiophenes in fuel under ambient conditions without special equipment requirements.[4–10] Early research on ODS or EDS mainly focused on exploring various traditional volatile organic solvents (such as formic acid and acetic acid as classic catalysts as well as acetonitrile, dimethyl sulfoxide, and *N*-methyl-2-pyrrolidonium as extraction solvents), which are extremely detrimental to solvent recovery and environmental protection.[11,12] Meanwhile, compared with ODS, the ability to handle fuel with high sulfur content using only EDS in single-stage liquid–liquid extraction is limited, which can result in additional operational expenses.[13,14] Moreover, highly polar ionic liquids have emerged as alternative solvents to further strengthen the desulfurization process by combining extraction and catalytic oxidation, ultimately achieving efficient desulfurization.[15–19] However, ionic liquids formed from completely ionized expensive substances through ionic bonds are limited for large-scale desulfurization because of their poor biodegradability and sustainability.[20–22] Therefore, the construction and design of novel alternatives with no need for purification and high self-degradation properties are attracting widespread interest.

Deep eutectic solvents (DESs), universally recognized as green functional solvents, exhibit tremendous potential in various applications owing to their superior physicochemical characteristics.[23–25] In general, DESs are obtained by mixing degradable and inexpensive hydrogen bond acceptors (HBAs, *e.g.*, quaternary salts or metal chlorides) with hydrogen bond donors (HBDs, *e.g.*, amines, acids, or alcohols) in a specific molar ratio, thereby generating a new homogeneous solvent with a melting point below that of either individual component.[26–28] No by-products are generated during their formation process, and the atomic utilization rate reaches 100%, allowing direct use of *in situ* synthesized DESs without the need for purification. While preserving key advantages of traditional ionic liquids, such as low vapor pressure and tunable chemical properties, DESs effectively overcome their aforementioned limitations related to synthesis mechanisms and material choices. Furthermore, through rational component selection, DESs that meet specific requirements and desired performance can be easily customized, such as in terms of their adjustable viscosity, polarity, and solvation ability.[27,29] The synergistic advantages of diversified composition and enriched internal hydrogen bonds[30,31] make DESs a promising candidate for effective extraction coupled catalytic oxidation. Notably, the design of acidic DESs, such as carboxylic acid- and sulfonic acid-based DESs, is the most effective strategy for achieving desulfurization, compared with the reported DESs because of their rich catalytic sites and excellent surface activity.[32–36] In our previous work, we developed inorganic–organic dual-acid DESs by combining the ionic liquid [BMIM]Cl with carboxylic acids (*e.g.*, formic acid and acetic acid) to enhance catalytic site density through Brønsted–Lewis acid synergy.[33,36] While these DESs demonstrated improved desulfurization efficiency, their recyclability was limited to ≤5 cycles owing to the volatility of organic acids and the high viscosity of ionic liquid-based systems. Furthermore, the catalytic mechanism was primarily attributed to acid strength rather than electronic structure modulation, leaving room for optimization in oxidant activation and stability.

To overcome these limitations, a paradigm shift was proposed from traditional acid-dominated DESs to coordination-regulated DESs by leveraging the unique properties of organic phosphonic acids. Compared with carboxylic acids, phosphonic acids exhibit stronger acidity, lower volatility, and exceptional coordination capability *via* their P═O groups.[37,38] These attributes enable the formation of stable metal-mediated coordination networks with metal chlorides (*e.g.*, $ZnCl_2$), which can regulate the electronic structure of catalytic sites to enhance oxidant activation.[39,40] Herein, we designed bifunctional phosphonic acid-based DESs (PDESs) using $ZnCl_2$ and aromatic phosphonic acids (phenylphosphinic acid, PIA; phenylphosphonic acid, POA) for the first time. By constructing hydrogen-bonding networks and electron transfer bridges between components, PDESs were found to act as extractants and catalysts in the reaction system. P═O···Zn coordination not only stabilized the PDES structure but also induced electron transfer to optimize Zn^{2+} sites for H_2O_2 adsorption and reactive oxygen radicals generation (*e.g.*, $^{\bullet}O_2^-$ and $^{\bullet}OH$). Under optimal reaction conditions, PDES $ZnCl_2$/2PIA could efficiently achieve ultradeep desulfurization with a desirable sulfur removal of 100% for heterocyclic thiophenes. These findings offer new insights into effective desulfurization and open up opportunities for other related application.

Results and discussion

Characterization of the PDES

The PDES $ZnCl_2$/2PIA was prepared through a one-pot method, in which the raw materials $ZnCl_2$ and PIA were mixed in a molar ratio of 1 : 2 (Fig. 1a). In general, the successful synthesis of a DES involves the reduction of the melting point and the formation of weak interactions such as hydrogen bonds.[28,30,41,42] The melting point of the as-prepared PDES, determined (−48.8 °C, Fig. 1b) using a differential scanning calorimetry (DSC), was much lower than that of its individual components ($ZnCl_2$ as 293 °C and PIA as 85 °C), indicating that there were interactions between $ZnCl_2$ and PIA. To qualitatively understand the site where $ZnCl_2$ interacted with PIA, the surface electrostatic potential analysis mapped on the total electron density with an isovalue of 0.001 was conducted (Fig. 1a). The red areas and the blue areas depicted in Fig. 1a represent the electron-rich regions and electron-deficient regions, respectively. Clearly, the negatively charged O atoms on the phosphoryl group (P═O) in PIA tend to interact with the positively charged Zn atom of $ZnCl_2$, and Cl atoms from $ZnCl_2$ tend to be closer to the H atoms of PIA. Meanwhile, ^{1}H NMR spectra using dimethyl sulfoxide-d6 as a deuterated solvent, and FT-IR spectra were implemented to further identify interactions and the structure of the PDES. The ^{1}H NMR spectrum of PIA exhibited four peaks at 11.15, 8.18, 7.74, and 6.82 ppm, while for the PDES, the peaks appeared at 8.68,

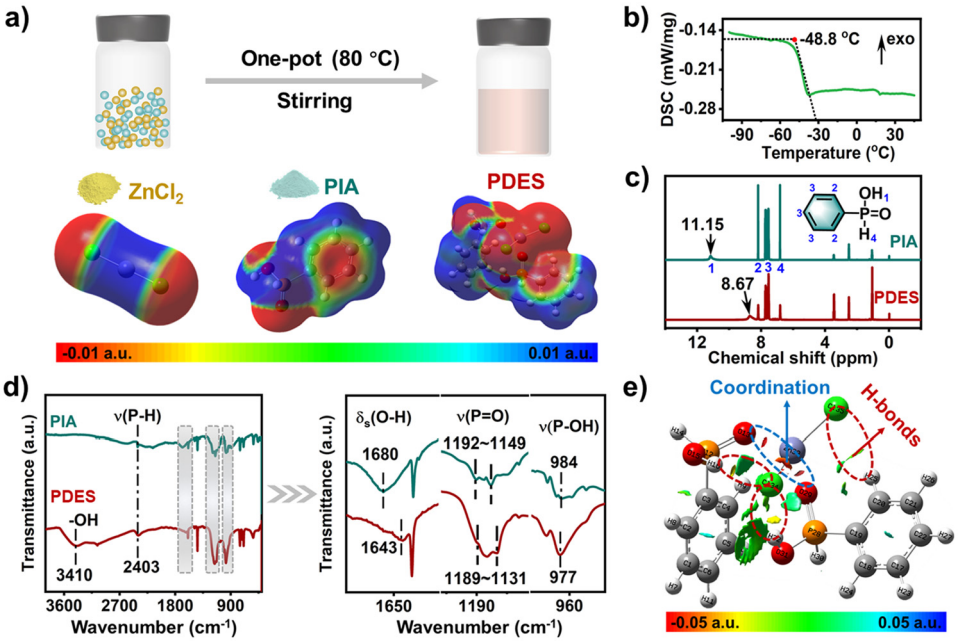

Fig. 1 (a) The synthesis of the PDES and electrostatic potential surface analysis for all the molecules mapped on the total electron density with an isovalue of 0.001. (b) The DSC curve of the PDES. (c) ^{1}H NMR and (d) FT-IR spectra of PIA and PDES. (e) Gradient isosurfaces (s = 0.35 a.u.) for PDES-1. The surfaces are colored on a red-green-blue scale according to sin(λ)ρ values, ranging from −0.05 to 0.05 a.u.

8.17, 7.74, and 6.80 ppm (Fig. 1c). A distinct shift in the hydrogen signal from 11.15 to 8.68 ppm was identified for P-OH, which was due to an increase in the electron cloud density on P-OH caused by the formation of intermolecular hydrogen bonds (–OH···Cl) between PIA and $ZnCl_2$. In Fig. 1d, representative characteristic peaks of PIA at 2403 cm^{-1} (stretching vibration peak of P–H), 1680 cm^{-1} (scissor bending vibration of O–H), 1192–1149 cm^{-1} (stretching vibration peak of P═O) and 984 cm^{-1} (stretching vibration peak of P-OH) can be observed for the as-prepared PDES.[43] Compared with PIA, a broader and stronger absorption peak belonging to the –OH group around 3410 cm^{-1} appears, and the redshift of δ_s(O–H) and ν(P-OH) peaks (from 1680 cm^{-1} to 1643 cm^{-1} and from 984 cm^{-1} to 977 cm^{-1}, respectively) were clearly observed for PDES, likely owing to the formation of hydrogen bonds.[44,45] The ν(P═O) peak exhibited a red shift, and the relative intensity decreased at 1192 cm^{-1} and 1149 cm^{-1}, suggesting that P═O was also involved in the formation of weak interactions.[46] In addition, specific interaction types within PDES $ZnCl_2$/2PIA were further identified through reduced density gradient (RDG) analysis using Multiwfn.[47,48] Firstly, the different configurations of the PDES were optimized, and the distance of intermolecular interactions is depicted by a dashed line (Fig. S1†). The configuration named as PDES-1 was the most stable owing to the lowest energy (ΔE = −82.65 kcal mol^{-1}). Then, the gradient isosurfaces (s = 0.35 a.u.) for PDES-1 were plotted in Fig. 1e. Red represents strong attractive interactions such as coordination, transition regions represent typical hydrogen bonding and van der Waals interactions, and blue represents non-bonding overlap regions. According to Fig. 1e, hydrogen bonding (O15–H16···Cl34 2.17 Å, O31–H32···Cl34 2.19 Å and C20–H25···Cl30 2.78 Å) and coordination (P28 = O29···Zn33 1.98 Å and P18 = O13···Zn33 1.99 Å) were responsible for the formation of PDES $ZnCl_2$/2PIA.

Evaluation of extraction and catalytic oxidation performance

To evaluate the extraction and catalytic performance of the PDESs, the removal of dibenzothiophene (DBT), which is widely present in residual oil, using 30 wt% aqueous hydrogen peroxide (H_2O_2) as the oxidant was conducted at a reaction temperature of 45 °C. As shown in Table 1, it is almost impossible to remove DBT using either $ZnCl_2$ or PIA alone (entries 1 and 2), and the solid mixture of $ZnCl_2$ + PIA with a molar ratio of 1 : 1 exhibited an ultra-low ECODS rate of 12.8% owing to

Table 1 DBT removal using PDESs with different components

Entry	PDESs	Molar ratio	EDS[a] Sulfur removal/ %	ECODS[b]	K_N	Viscosity[c] (P)
1	$ZnCl_2$	—	1.8	4.8	—	—
2	PIA	—	2.4	3.4	—	—
3	$ZnCl_2$ + PIA[d]	1 : 1	4.3	12.8	0.16	—
4	$ZnCl_2$/PIA	1 : 1	27.8	96.4	1.39	21.4
5	$ZnCl_2$/2PIA	1 : 2	36.4	100	2.06	14.6
6	$ZnCl_2$/3PIA	1 : 3	24.5	89.3	1.17	29.4
7	2$ZnCl_2$/PIA	2 : 1	11.6	64.2	0.47	89.9

Reaction conditions: m (PDES) = 1 g, V (model fuel) = 5 mL, and T = 45 °C. [a] t = 15 min. [b] O/S = 3, t = 45 min [c] The temperature of viscosity for PDESs is 45 °C. [d] Solid mixture of $ZnCl_2$ and PIA.

insufficient affinity with DBT and limited active sites (entry 3). Notably, when the $ZnCl_2$/PIA PDES formed *via* a one-pot method in the same molar ratio was introduced into the reaction system, extraction and catalytic performance simultaneously enhanced. As a result, DBT removal significantly improved, with EDS and ECODS reaching 27.8% and 96.4%, respectively. Besides $ZnCl_2$/PIA, PDESs with different molar ratios of $ZnCl_2$ to PIA (Z/P = 1 : 2, 1 : 3, and 2 : 1) were investigated to screen the most ideal composition. It could be unveiled from Table 1 that DBT removal significantly reduced as the feed $ZnCl_2$ content increased (entries 4 and 7), while a volcano-type trend of DBT removal was observed as the PIA content increased (entries 4, 5 and 6). A notable observation was the different fluidities of the above synthesized PDESs; therefore, the viscosity was accurately measured using viscometry. As shown in Table 1, $ZnCl_2$/2PIA (Z/P = 1 : 2) with the lowest viscosity value (14.6 P) exhibited the strongest mass transfer ability in the ECODS system compared with other synthesis ratios of the PDES. The DBT removal and Nernst distribution coefficient (K_N) values using the bifunctional PDES $ZnCl_2$/2PIA as an extractant and catalyst reached their maximum value, wherein the extraction and conversion rates were 36.4% and 100%, respectively.

Numerous published reports have shown that Zn^{2+} plays a key role in catalytic activation using DESs or ionic liquids containing $ZnCl_2$ as catalysts in the ODS process,[13,49–51] but the underlying mechanism was not explained. Herein, besides PIA, two other types of $ZnCl_2$-PDESs were synthesized based on phosphoric acid (PA) and POA at a mass ratio of 1 : 2 (Fig. 2a) to explore the essence of catalysis in the PDES-ODS system. Compared with the activity of each individual component (PIA 3.4%, PA 6.2% and POA 4.1%) in Table S1,† the catalytic activity of these prepared PDESs, $ZnCl_2$/2PIA, $ZnCl_2$/2PA and $ZnCl_2$/2POA, was significantly enhanced (Fig. 2b), which might be related to the formation of internal coordination interactions. It was clearly observed from the structural analysis (Fig. 1) that there was a special coordination (P═O···Zn) within the PDES in addition to common hydrogen bonds, which might be the key to inducing a change in the electronic interaction of Zn^{2+} for promoting catalytic activation. To explain this hypothesis, all possible optimized $ZnCl_2$-PDESs based on PIA, PA and POA were first evaluated through DFT calculations (Fig. S2 and S3†). Interestingly, among the three most stable PDES models selected, coordination (P═O···Zn) occurs between the Zn atom of $ZnCl_2$ and the O atom of P═O (Fig. 2c). Meanwhile, through natural population charge (NPA) analysis of the Zn atom and the O atom of in P═O in the PDESs, it was found that the three optimal PDES exhibited a strong the bond order of O···Zn (≥0.214), and the charge of Zn increased because of coordination induction (Table S2†). Furthermore, different models of $ZnCl_2$/2PIA, $ZnCl_2$/2PA and $ZnCl_2$/2POA combined with the oxidant H_2O_2 were constructed and optimized to investigate the catalytic activity of $ZnCl_2$-PDES regulated by the electronic structures of various phosphoric acid compounds (Fig. S4–S6†). Interestingly, the interaction energies of $ZnCl_2$/2PIA, $ZnCl_2$/2PA, and $ZnCl_2$/2POA with the oxidant H_2O_2 were 30.06 kcal mol^{-1}, 26.03 kcal mol^{-1}, and 27.58 kcal mol^{-1}, respectively, which were much higher than that of $ZnCl_2$ (15.79 kcal mol^{-1}, Fig. S7†). The above results confirmed that the coordination construction of the $ZnCl_2$-PDES improved the electronic interaction of Zn^{2+}, positively affecting the adsorption and activation of H_2O_2. Furthermore, the spectral analysis and catalytic performance of the PDES with varying $ZnCl_2$/PIA molar ratios (x = 0.2, 0.4, 0.6, 0.8, and 1) further revealed that $ZnCl_2$ in the PDES regulates the Zn^{2+}'s electronic structure *via* coordination, optimizing H_2O_2 adsorption/activation while forming a low-viscosity system for efficient mass transfer (Fig. S8†).

In addition, compared with $ZnCl_2$/2PA (which lacks benzene rings), $ZnCl_2$/2PIA and $ZnCl_2$/2POA (which contain benzene rings) demonstrated stronger catalytic oxidation ability (Fig. 2b). This might be attributed to the conjugation effect of the benzene ring, which lowered the force constant of the phosphoryl group (–P═O), thereby promoting electron transfer from O to Zn. To confirm this hypothesis, the charge of Zn for $ZnCl_2$/2PIA, $ZnCl_2$/2PA and $ZnCl_2$/2POA was calculated, as shown in Fig. 2c and Table S2.† $ZnCl_2$/2PIA and $ZnCl_2$/2POA exhibited charge change values of Zn of 0.040 and 0.034, respectively, which were much higher than that of $ZnCl_2$/2PA (0.016) (which lacks benzene rings), indicating that the presence of benzene rings could further enhance the electronic regulation of Zn, thereby promoting the catalytic ODS performance of PDESs.

Apart from the internal electronic structure, the physical properties of the bifunctional PDESs $ZnCl_2$/PIA and $ZnCl_2$/POA, such as viscosity and acidity, are important factors affecting ECODS. The DBT removal rate using $ZnCl_2$/POA with high viscosity (32.8 P) was significantly lower than that using $ZnCl_2$/PIA (14.6 P) under the same reaction conditions (Fig. 2b). Meanwhile, the contribution of their acidity to catalytic performance was investigated through UV-Vis spectroscopy using 4-nitroaniline ($pK(I)_{aq}$ = 0.99) as an indicator (Table S3† and Fig. 2d). It is universally known, based on the Hamiltonian acidity function (H_0), that the smaller the value of H_0, the stronger the acidity. The result in Fig. 2d shows that the acidity of the PDES $ZnCl_2$/PIA was stronger, which was beneficial for the activation of H_2O_2, thus accelerating the oxidation removal of DBT.[35,52,53]

Desulfurization performance under different variables

The above results demonstrated that the bifunctional PDES $ZnCl_2$/2PIA by inducing strong electronic interaction *via* coordination regulation showed the most remarkable desulfurization performance, and therefore, it was used to implement a series of control experiments to investigate the influence of different reaction conditions on sulfur removal. Firstly, an experimental design based on the $L_9(3^4)$ orthogonal array was established to determine the primary and secondary factors affecting desulfurization.[54,55] As shown in Tables S4 and S5,† the investigated parameters include reaction temperature, the dosage of the $ZnCl_2$/2PIA PDES and the molar ratio of the oxidant to sulfide (O/S). The orthogonal experiments were con-

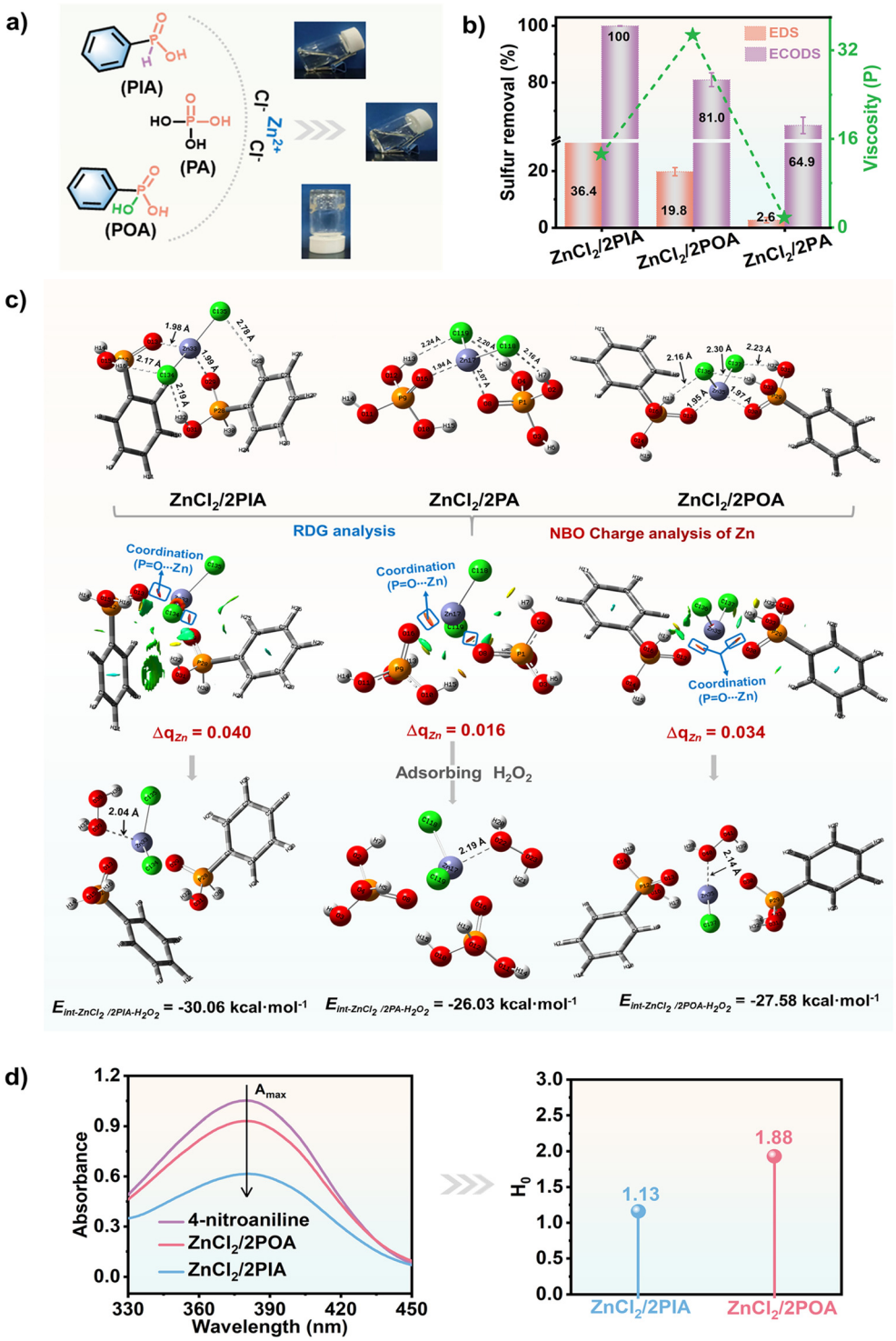

Fig. 2 (a) Schematic of PDES 2X/$ZnCl_2$ (X = PIA, PA, and POA) synthesis. (b) The relationship between extraction/catalytic performance and viscosity. (c) Gradient isosurface (s = 0.35 a.u.) of optimal PDESs, and adsorption energy analysis with the H_2O_2 oxidant. (d) Hammett function calculation using 4-nitroaniline ($pK(I)_{aq}$ = 0.99) as the indicator.

ducted as per the conditions mentioned in Table S4,† and 12 sets of DBT conversion rates were measured (Table S5†) to obtain the variance, significance coefficient P value, and optimization range R value between the selected factors and sulfur removal (Table S6 and Fig. S9†). Through the analysis of the above results, it was concluded that among the three influencing factors, the O/S had the minimal impact on the conversion of DBT, whereas the reaction temperature had the greatest

impact. The P value between the optimized reaction temperature and desulfurization rate was 0.025, which was much lower than the standard value ($P < 0.05$), and the significant relationship between the two was the strongest. Thus, it was concluded that as the reaction temperature increased, the conversion of DBT improved, and the optimal temperature could be further determined through comparative experiments.

Generally, as a special exothermic-endothermal integrated reaction, ECODS benefits from moderate reaction temperature.[4,56–58] As shown in Fig. 3a, the extraction-based DBT removal efficiency without an oxidant first increased and then decreased (21.2% to 36.4% to 31.7%) as the temperature varied from 25 °C to 65 °C within 15 min. Since extraction is an exothermic process, high temperature was not conducive to DBT extraction, while the high viscosity of the PDES at a lower temperature (Fig. S10†) limited the mass transfer within the reaction system. Notably, with the addition of the oxidant, the DBT removal performance significantly improved and catalytic efficiency gradually enhanced as the temperature increased. Specifically, the oxidation-based removal of DBT reached 99.3% within 90 min when the temperature was 25 °C, while it only took 45 min to achieve 100% deep desulfurization as the temperature was increased to 45 °C. Although the catalytic activity of the PDES for DBT removal was slightly promoted as temperature was further raised to 55 and 65 °C, the partial self-decomposition of 30 wt% H_2O_2 as the oxidant and the cost of excessive energy consumption should be given special attention. As a consequence, 45 °C was considered the optimal temperature for ECODS in which the extraction (36.4%) and conversion of DBT (100%) were the most feasible and economical. To better explain the oxidation of DBT, reaction kinetics as the primary parameter were calculated. As presented in Fig. S11a,† the studied ECODS system displayed a linear relationship between time and $\ln(C_0/C_t)$, which was well fitted to the pseudo-first-order kinetic model. Notably, the reaction rate constants for DBT oxidation increased from 0.027 to 0.169 min^{-1} with the reaction temperature increasing from 25 to 65 °C, further proving that a high reaction temperature is beneficial to the ECODS reaction. Moreover, according to the linear relationship between $1000/T$ and $-\ln k$, the activation energy (E_a) for DBT oxidation was found to be 38.8 kJ mol^{-1} (Fig. S11b†).

The added amount of the oxidant is another prominent and decisive factor of ODS. Usually, on the premise of ensuring no loss of the oxidant, 1 mol of sulfur in DBT to be completely oxidized requires at least 2 moles of oxygen. Herein, the effect of different molar ratios of oxygen to sulfur (O/S = 2, 3, 4, and 5) on DBT conversion was explored using the $ZnCl_2$/2PIA PDES as the catalyst and H_2O_2 as the oxidant, and the results are shown in Fig. S12.† After 60 min of the reaction, the desulfurization efficiency of $ZnCl_2$/2PIA gradually enhanced from 86.9% to 100% by slightly increasing the O/S from 2 to 3. Interestingly, the complete removal of DBT could be observed when the reaction time was extended to 90 min under an O/S of 2. These results might provide compelling evidence for the positive role of $ZnCl_2$/2PIA in promoting the production of clean fuel. Apart from this, the effect of PDES dosage on DBT removal performance was studied (Fig. S13 and S14†). In the blank ODS process without the PDES, DBT could hardly be oxidized with an ultra-low desulfurization rate of 6.8%. It was

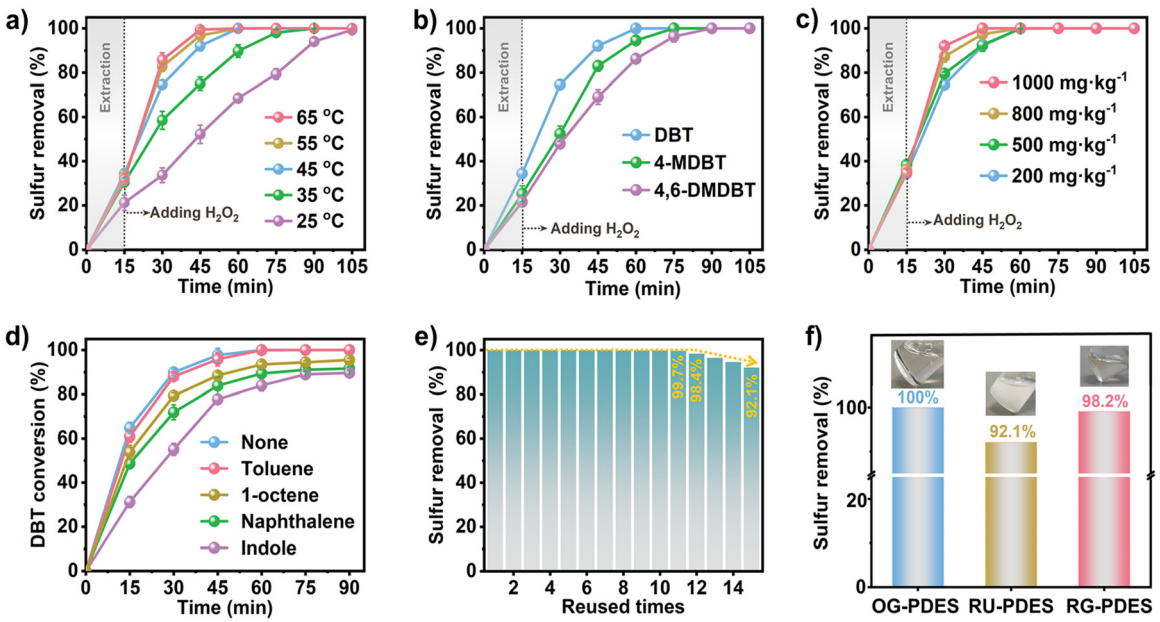

Fig. 3 (a) Desulfurization performance evaluation of the $ZnCl_2$/2PIA PDES at different reaction temperatures. (b) Extraction selectivity and catalytic oxidation activity for different sulfur-containing substances. (c) Effect of different sulfur concentrations on the ECODS performance of the DES. (d) Effect of interfering agents on DBT conversion. (e) Recycling and (f) regeneration performance. OG-PDES, RU-PDES, and RG-PDES refer to the original PDES, the reused PDES, and the regenerated PDES, respectively.

worth noting that adding only 0.25 g of the PDES triggered desulfurization, with the DBT removal efficiency significantly increasing from 54.2% to 86.3% within 60 min with an increase in PDES dosage from 0.25 to 0.5 g. It could be concluded that the amount of the PDES was directly proportional to the extraction and catalytic performance of the PDES. When the added amount of the PDES was 1.0 g, the catalytic activity of the PDES was close to saturation, and ultradeep desulfurization (100%) could be achieved (Fig. S14†).

Considering the complexity, diversity and uncertainty of the sulfide types and sulfur content in actual diesel fuel, it is necessary to investigate the removal efficiency of alkyl-substituted dibenzothiophenes, including 4-MDBT and 4,6-DMDBT, that are more difficult to remove, besides DBT. As shown in Fig. 3b, the PDES exhibited stronger ability to separate DBT from oil with an extraction rate of 36.4%, and the sequence of oxidation removal for the selected typical sulfides is as follows: DBT > 4-MDBT > 4,6-DMDBT. The difference in the selectivity and catalytic activity of the PDES towards substrates was mainly caused by electron affinity and steric hindrance on the S atom.[59–61] Specifically, compared with DBT, the presence of methyl groups in 4-MDBT and 4,6-DMDBT formed a stronger steric hindrance effect, resulting in a significant reduction in the accessibility of active sites and S atoms, further hindering catalytic activation. Interestingly, the removal of all sulfur-containing substrates was as high as 100% under identical reaction conditions, clearly demonstrating that the bifunctional PDES $ZnCl_2$/2PIA could effectively overcome the negative impact of methyl steric hindrance to achieve efficient ultradeep desulfurization of fuel. In addition, the effect of various sulfur contents (200 mg kg^{-1}, 500 mg kg^{-1}, 800 mg kg^{-1} and 1000 mg kg^{-1}) in model oil containing DBT as a specific substrate on the desulfurization performance of the PDES was investigated. As depicted in Fig. 3c, it was found that the extraction ability of the PDES was almost unaffected, while the reaction time of catalytic ODS was significantly shortened with an increase in the initial sulfur content. The residual sulfur content sharply decreased from 1000 mg kg^{-1} to 2 mg kg^{-1} in only 30 min, resulting from an enrichment in reactant (DBT and H_2O_2) concentrations within the PDES-ECODS system. Furthermore, aromatics, olefins and aromatic nitrides, as typical interfering substances in actual diesel fuel, exert significant impact on the selective removal of sulfides. Herein, toluene, 1-octene, naphthalene and indole, as representative interferents, were added to the reaction, to explore their influence on desulfurization activity (Fig. 3d and Fig. S15†). It was observed that the addition of the aforementioned interferents in the PDES-CODS reaction demonstrated minimal or no effect on the removal capacity of DBT by the PDES, further proving the high selectivity and catalytic activity of $ZnCl_2$/2PIA for potential applications in cleaning actual fuels.

Besides providing excellent desulfurization performance, the reusability and stability of the PDES constitute the main index to evaluate its practical application. Spectral analysis of the PDES and dodecane solvent in fuel before and after mixing clearly illustrated that the PDES and the fuel were immiscible (Fig. S16 and S17†). The PDES could be separated from the clean fuel after the reaction *via* decantation. As displayed in Fig. 3e, the PDES demonstrated excellent sustainability, maintaining a DBT removal rate of 98.4% even after the 12th cycle without any treatment. Thereafter, with a continued increase in the number of cycles, DBT removal efficiency gradually decreased under the same conditions, and a large amount of white oxidation products accumulated in the PDES phase (Fig. 3f). Moreover, the used PDES could be regenerated by washing with deionized water, followed by drying (Fig. S18†). The catalytic activity of the regenerated PDES was restored, and the DBT removal rate increased from 92.1% to 98.2% (Fig. 4f), revealing the high stability and durability of the bifunctional $ZnCl_2$/2PIA PDES against the complex reaction. As shown in Table 2 and Table S7,† the $ZnCl_2$/2PIA as a promising extractant and catalyst outperforms other DESs in achieving clean fuel production.

Analysis of DES-ECODS products

After continuous multiple oxidation reactions, white products formed and accumulated in the used PDES. The spectrum given in Fig. 4a shows the skeleton structure fluctuation of the recovered oxidation product obtained through ordinary cleaning techniques such as filtration, washing and drying, in

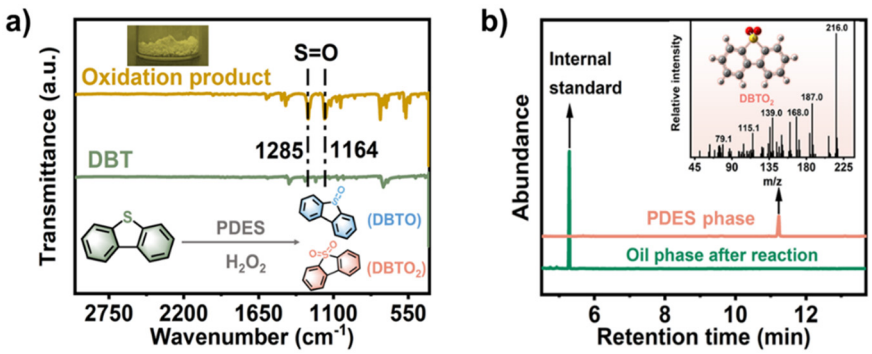

Fig. 4 (a) FT-IR spectra of the oxidation product. (b) GC-MS spectra of the main compounds in the reacted oil phase and PDES catalyst phase. Reaction conditions: *m* (PDES) = 1.0 g, *V* (model fuel containing DBT, 200 mg kg^{-1}) = 5 mL, *T* = 45 °C, and O/S = 3.

Table 2 Comparison of DBT removal performance of different DES-ECODS systems

DESs	Reaction conditions			Cycle index	ECODS (%)	Ref.
	O/S	T (°C)	t (min)			
$ZnCl_2$/2PIA	3	45	45	11	100	This work
L-Pyro/TFA	3	60	180	3	99.7	62
L-Pro/*p*-TsOH	5	60	120	6	99	63
$C_3H_6O_2$/ 0.5$ZnCl_2$	4	30	180	5	99.42	64
C_2H_5NO/3*p*-TsOH	5	50	120	6	100	65
MBCD/3FA	3	60	240	4	99.9	66
TBAB/PEG-200	8	40	75	7	99.65	67
[PSTEtA]Cl/AA	5	50	180	5	95.1	68
ChCl/ 1.5CF_3SO_3H	6	40	60	5	98.65	69

L-Pyro = L-pyroglutamic acid, TFA = trifluoracetic acid, *p*-TsOH = *p*-toluenesulfonic acid, L-Pro = L-proline, $C_3H_6O_2$ = propionic acid, C_2H_5NO = acetamide, MBCD = methyl-β-cyclodextrin, FA = formic acid, TBAB = tetrabutylammonium bromide, PEG-200 = polyethylene glycol-200, [PSTEtA]Cl = (3-sulfopropyl)triethylammonium chloride, AA = acetic acid, and ChCl = choline chloride.

which two prominent peaks ascribed to the stretching vibration of S=O appeared at 1164 cm^{-1} and 1285 cm^{-1} compared with DBT. These peaks indicated the presence of polar sulfoxide (DBTO) or sulfone ($DBTO_2$) with high added value in the recovered product. To gain a more accurate identification of the product type in the oxidation process, gas chromatography-mass spectrometry (GC-MS) was employed (Fig. 4b and Fig. S19†). In Fig. S19,† only DBT could be detected in the pristine fuel. The $ZnCl_2$/2PIA PDES phase after the reaction was subjected to extraction using carbon tetrachloride (CCl_4) and then analyzed through GC-MS. As the reaction proceeded, the peak attributed to DBT in the fuel gradually decreased and eventually disappeared around 7 min, while a strong peak appeared in the PDES phase at about 11.3 min (Fig. 4b). By identifying molecular fragments, it could be concluded that the corresponding substance structure of this peak with an m/z of 216.0 was $DBTO_2$, indicating the excellent catalytic activity of $ZnCl_2$/2PIA and that DBT was completely oxidized to sulfone ($DBTO_2$) in the PDES-CODS system.

Proposed mechanism

The reaction mechanism plays a crucial role in the optimization of the desulfurization process and in designing effective extractants or catalysts. The extraction and catalytic oxidation mechanisms of the bifunctional $ZnCl_2$/2PIA PDES were systematically investigated through experiments, characterizations, and DFT calculations. Firstly, FT-IR and ^{1}H NMR spectroscopy were implemented to gain a preliminary insights into the fundamental nature of the interaction between the PDES and DBT during extraction. As shown in Fig. 5a, attenuation bands of DBT in the mixture (PDES + DBT) at 733 cm^{-1} and 700 cm^{-1}

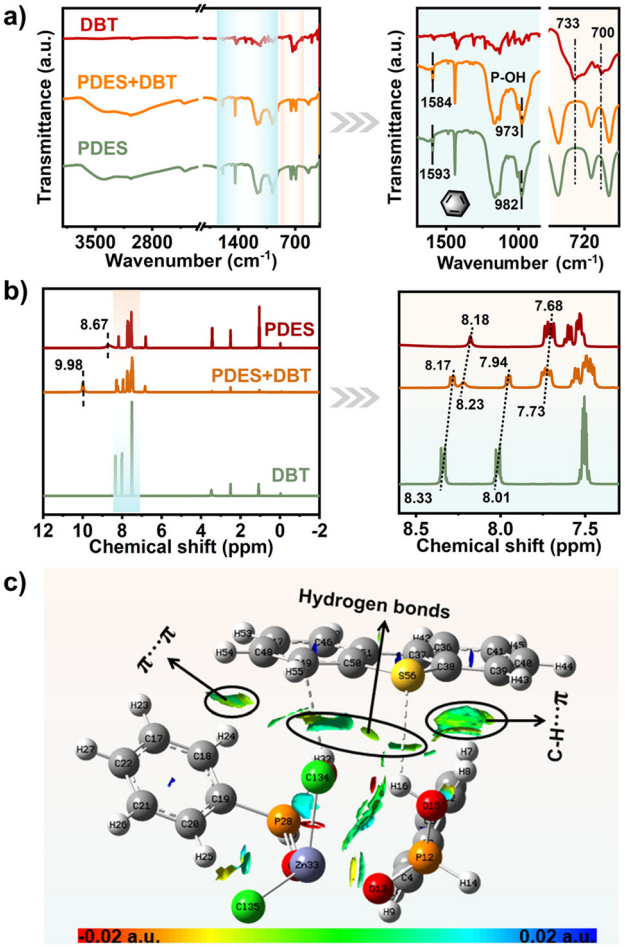

Fig. 5 (a) FT-IR and (b) ^{1}H NMR spectra of the product obtained from the reaction between the PDES and DBT. (c) Gradient isosurfaces (s = 0.35 a.u.) for the optimized structure of PDES-1–DBT-1. The surface is colored on a red-green-blue scale, according to the value of $\sin(\lambda)\rho$, ranging from −0.02 to 0.02 a.u.

indicated a strong interaction between the PDES and DBT, leading to a decrease in the quasi-aromaticity of DBT.[70] The chemical environment of the active hydrogen in the PDES underwent significant changes after interacting with DBT (Fig. 5b). Specifically, the shorter and broader peak at 8.67 ppm shifted downfield to 9.98 ppm, becoming sharper and more prominent in shape. The reason was that the hydrogen bonding (–OH···Cl) of the PDES was likely disrupted upon the addition of DBT, causing active hydrogen to preferentially interact with the S atom in DBT. This interaction further enhanced the electron-withdrawing ability of the hydrogen atoms on the thiophene ring of DBT, resulting in a decrease in hydrogen nuclear electron density.[71] The pronounced downfield shift in the active hydrogen peaks of DBT at 8.33 ppm and 8.01 ppm interacting with the PDES, accompanied by a decrease in peak intensity, precisely supported this viewpoint. In addition, the corresponding hydrogen signals on the benzene ring of the PDES shifted from 8.18 and 7.68 ppm to 8.23 and 7.73 ppm, respectively, indicating that there might be

other interactions between the PDES and DBT besides hydrogen bonds.

The interaction types were also visualized and recorded through theoretical calculations. Firstly, new models for $ZnCl_2$, PIA, and PDES-1 combined with DBT were constructed and optimized to obtain their most stable structures (Fig. S20–S22†). By comparing the interaction energy, it was observed that the extraction energy of the PDES for DBT was much higher than that of PIA and $ZnCl_2$, especially PDES-1-DBT-1 with a ΔE_{int} as high as 21.68 kcal mol^{-1}. Meanwhile, the obtained gradient isosurface (s = 0.35 a.u.) of the optimized structures using the RDG method was plotted (Fig. 5c and Fig. S23†). Notably, in addition to hydrogen bonds, the strong extraction performance of the PDES-ECODS reaction system benefited from the π···π interaction and C–H···π interaction between the benzene ring of the PDES and DBT.

During the catalytic oxidation process, reactive oxygen species were examined by incorporating various radical scavengers into the reaction system. $AgNO_3$, benzoquinone (BQ), and *tert*-butanol (TBA) were selected as effective scavengers for e^-, $^{\bullet}O_2^-$ and $^{\bullet}OH$, respectively. As shown in Fig. 6a, the addition of $AgNO_3$ had almost no effect on the oxidation-based removal of DBT. However, when a moderate amount of TBA or BQ was added to the PDES-ODS system, the ODS performance of the PDES was suppressed, resulting in DBT conversion rates of 53.4% and 41.7%, respectively. When BQ and TBA were simultaneously introduced, the DBT removal rate dropped from 100% to 33.1%, indicating that $^{\bullet}O_2^-$ and $^{\bullet}OH$ radicals are actively involved in the oxidation process. Furthermore, the reactive oxygen species generated during the activation of H_2O_2 by the PDES were recorded using ESR spectroscopy with 5,5-dimethyl-1-pyrroline *N*-oxide (DMPO) as the spin trapping agent (Fig. 6b). The results showed the detection of two distinct quadruplet structures (1 : 1 : 1 : 1 and 1 : 2 : 2 : 1), corresponding to DMPO-$O_2^{\bullet-}$ and DMPO-$HO^{\bullet}$.

^{1}H NMR spectroscopy is often used to explore peroxide species in the oxidation reaction owing to its sensitivity to acidic groups and active hydrogen. As shown in Fig. 6c, the signal at 8.67 ppm attributed to the active hydrogen of –POOH in $ZnCl_2$/2PIA underwent a significant change after the reaction of the PDES with H_2O_2. Compared with the pure PDES, the hydrogen signal shifted to a higher field for PDES + H_2O_2, with the peak becoming stronger and narrower. This was attributed to the shielding effect resulting from the formation of peroxides,[72] indicating a strong interaction between the PDES and H_2O_2. Additionally, it should not be ignored that the hydrogen signal at 6.31 ppm downshifted to 6.45 ppm after extending the reaction by 30 min. This was primarily because the oxygen atom connected to the active hydrogen in –POOH exhibited strong electrophilicity, leading to a decrease in the electronic density of the hydrogen atom.[11,33] Based on the existing results and previous research,[52,53] the structure of hyperoxide (PDES-OOH) formed by the PDES and H_2O_2 is shown in Fig. 6d. PDES-OOH, as a precursor in the oxidation reaction, was also a potential reactive oxygen species for DBT oxidation.

According to the results from the above experiments, characterization, and theoretical calculations, a possible reaction mechanism underlying the ECODS by the bifunctional $ZnCl_2$/2PIA PDES is proposed (Scheme 1). Firstly, DBT was extracted from the oil phase into the PDES phase owing to the strong interactions between the PDES and DBT (*e.g.* hydrogen bonding, π···π and C–H···π interactions). Simultaneously, the H_2O_2 oxidant was activated by the PDES to form reactive oxygen species with stronger oxidation ability. DBT extracted into the PDES phase was further oxidized to $DBTO_2$ and retained in the PDES phase, ultimately affording a sulfur free clean fuel.

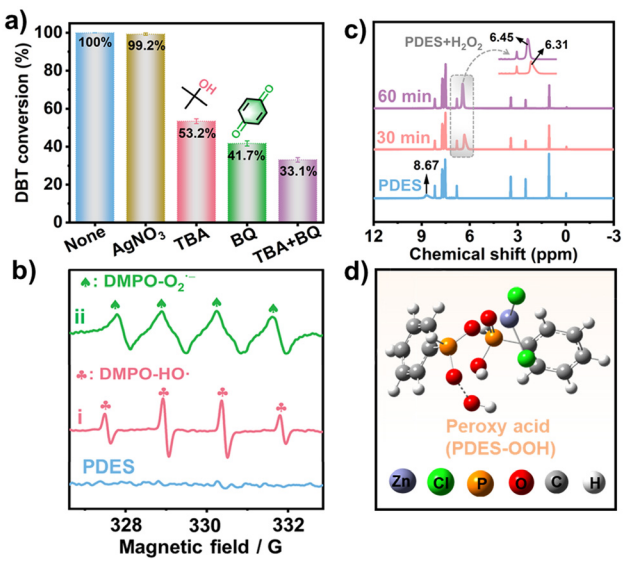

Fig. 6 Reaction mechanism for the catalytic oxidation process. (a) Selective quenching experiments and (b) ESR spectroscopy for the identification of reactive radicals; i and ii: PDES reacts with H_2O_2 for 10 min in deionized water and methanol as solvents. (c) ^{1}H NMR spectra of the reaction between the PDES and H_2O_2 for 30 min and 60 min. (d) Possible structure of peroxy acid (PDES-OOH).

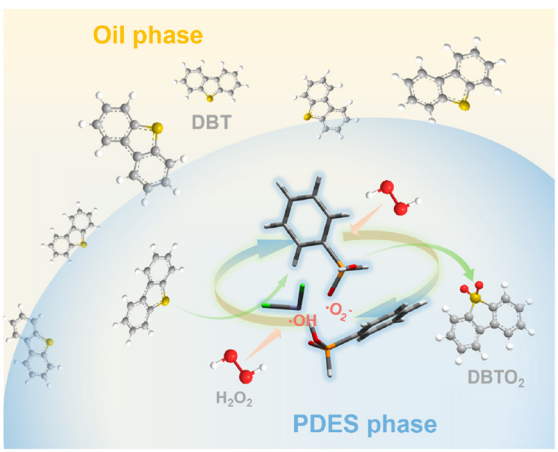

Scheme 1 ECODS mechanism using the bifunctional PDES $ZnCl_2$/2PIA.

Conclusions

In summary, a series of bifunctional PDESs based on organic phosphonic acids were successfully constructed *via* a one-pot method and employed for ECODS. Through the construction of hydrogen bonding networks and coordination electron induction, PDESs acted as extractants and catalysts and showed better catalytic activities caused by the electronic structure regulation of Zn^{2+} sites by the P═O groups in organic phosphonic acids. Among them, the $ZnCl_2$/2PIA PDES, containing strong electron transfer capability and high adsorption energy for the oxidant, could be reused for at least 12 times without any further treatment in the ECODS process, showing state-of-art cycle-regeneration stability. Moreover, the PDES could efficiently achieve ultradeep desulfurization with a desirable sulfur removal of 100% under mild conditions, which is also much higher than that of previously reported DESs. Results based on experimental and theoretical analyses indicated that the coordination constructed within PDESs can enhance the electronic interaction of Zn^{2+} sites, thereby inducing the catalytic activation of H_2O_2, in which $^{\bullet}O_2^-$ and $^{\bullet}OH$ were the main active reactive oxygen species, and peroxy acid (PDES-OOH) might also participate in the reaction. The $ZnCl_2$/2PIA PDES could adsorb surrounding sulfides *via* hydrogen bonding, π···π interactions and C–H···π interactions, enabling sulfides to permeate its phase, and further oxidized to $DBTO_2$ in the presence of the H_2O_2 oxidant. This work may provide a new strategy for the design of catalysts and extractants with low energy consumption.

Experimental

Preparation and characterization of a bifunctional PDES

All PDESs were synthesized using a simple one-pot method. Herein, the synthesis process for only the $ZnCl_2$/2PIA PDES is discussed (Fig. 1a) as the other PDESs were prepared *via* the same process. $ZnCl_2$ as a hydrogen bond acceptor and PIA as a hydrogen bond donor were added to a reaction vessel in a 1 : 2 molar ratio, and the solid mixture was stirred for 3–4 h under oil bath heating at 80 °C until a homogeneous liquid formed. The PDES structure was identified through Fourier transform infrared spectrometry (FT-IR, Nicolet 380, USA), ^{1}H-nuclear magnetic resonance spectra (^{1}H-NMR, Brucker ARX-400 Advance Spectrometer, Germany) and density functional theory (DFT) calculation. Differential scanning calorimetry (DSC) analysis was performed to explore the melting point of PDESs in the range of −100 °C–50 °C at a rate of 10 °C min^{-1}. Viscosity and acidity were also measured using a viscometer (IKA, ROTAVISC me-vi Complete) and ultraviolet-visible absorption spectroscopy (UV-Vis).

Desulfurization procedure

Different model oils comprising 200, 500, 800 and 1000 mg kg^{-1} dibenzothiophene (DBT) in *n*-dodecane with tetradecane as an internal standard were prepared to investigate the desulfurization performance of the PDES. In addition to DBT, 4-methyldibenzothiophene (4-MDBT,) and 4,6-dimethyldibenzothiophene (4,6-DMDBT) were selected as heterocyclic sulphides to simulate the environment of real diesel fuel. The typical desulfurization experiment was operated at 45 °C. First, 1 g of the $ZnCl_2$/2PIA PDES and 5 mL of model oil were first added into a customized reaction vessel, followed by vigorous stirring for 30 min to investigate the extraction desulfurization performance. Then, 9.6 μL of H_2O_2 (30 wt%) was injected into the system, and the sulfur content in the oil phase after the reaction was periodically analysed *via* gas chromatography equipped with a flame ionization detector. The sulfur removal percentage and Nernst partition coefficient (K_N) of the PDES-ECODS reaction system were calculated using eqn (1) and (2), respectively, where C_0 is the original sulfur content in the model oil, and C_t is the sulfur content after reaction over a period of time (t min).

$$\text{Sulfur removal } (\%) = (C_0 - C_t/C_0) \times 100 \quad (1)$$

$$K_N = [\text{mg(EDS) g}^{-1}\text{(PDESs)}]/[\text{mg(EDS) g}^{-1}\text{(oil)}]. \quad (2)$$

DFT calculations

All calculations, including the structural optimization of the PDES, the interaction between the PDES and DBT and the potential reaction energy in the catalytic ODS process, were carried out through the Gaussian 16 program using the M06-2X computational model with the B3LYP/6-31g (d,p) basis set level.[73,74] Frequency calculations and dispersion correction were performed at the same level to eliminate virtual frequency interference and estimate the basis set superposition error (BSSE). For all structures that guaranteed local minima, there was no imaginary frequency. In order to better understand the formation mechanism of the bifunctional PDES and the interaction between aromatic sulfur compounds, especially DBT, and the PDES, electrostatic potential analysis and reduced density gradient (RDG) analysis were performed.[73,75,76] Taking the formation of the $ZnCl_2$/2PIA PDES as an example, the interaction energy was calculated using eqn (3). The interactions between the PDES and aromatic sulfur compounds were evaluated using similar methods. In this regard, E_{PDES}, E_{ZnCl_2} and E_{PIA} represent the optimized energy of the PDES, $ZnCl_2$ and PIA, respectively. ΔE_{int} is the interaction energy between $ZnCl_2$ and PIA. The value of ΔE_{int} is usually negative. Notably, the more negative the value of ΔE_{int} is, the stronger the interaction between them.

$$\Delta E_{int} = E_{PDES} - E_{ZnCl_2} - E_{PIA} + E_{BSSE} \quad (3)$$

Author contributions

Lixian Xu performed conceptualization, validation, formal analysis, investigation, data curation, visualization, writing – original draft, and writing – review & editing; Jie Yin performed conceptualization, formal analysis, and writing – review &

editing; Dongao Zhu performed formal analysis and writing – review & editing; Beibei Zhang performed conceptualization, methodology, and supervision; Linhua Zhu performed supervision and writing – review & editing; Hongping Li performed software analysis, formal analysis, and supervision; Jing He performed formal analysis, supervision, and writing – review & editing; Huaming Li performed supervision and writing – review & editing; Wei Jiang performed conceptualization, formal analysis, supervision, project administration, funding acquisition, and writing – review & editing.

Data availability

The data that support the findings of this study are available from the corresponding author upon reasonable request.

Conflicts of interest

The authors declare no conflict of interest.

Acknowledgements

The authors are grateful for the National Natural Science Foundation of China (No. 22378176 and 22202088), the Jiangsu Funding Program for Excellent Postdoctoral Talent (2022ZB636) and Key Research and Development Project of Hainan Province (ZDYF2022GXJS330).

References

1 J. Zou, Y. Lin, S. Wu, Y. Zhong and C. Yang, *Adv. Funct. Mater.*, 2021, **31**, 2100442.
2 G. Ye, H. Wang, W. Chen, H. Chu, J. Wei, D. Wang, J. Wang and Y. Li, *Angew. Chem., Int. Ed.*, 2021, **60**, 20318–20324.
3 X. An, W. Jiang, L. Zhu, L. Xu, J. She, J. He, W. Zhu and H. Li, *Appl. Catal., B*, 2023, **333**, 122779.
4 G. Ye, G. Shi, H. Chen, L. Nie, Q. Zhang, L. Wu, J. Zhou and J. Wang, *Adv. Funct. Mater.*, 2024, 2014025.
5 J. Yin, W. Fu, J. Zhang, X. Zhang, W. Qiu, W. Jiang, L. Zhu, H. Li and H. Li, *Chem. Eng. J.*, 2024, **492**, 152349.
6 J. Xiong, J. Li, C. Chen, W. Jiang, W. Zhu, H. Li and J. Di, *Appl. Catal., B*, 2022, **317**, 121714.
7 L. Xu, J. Yin, Y. Luo, H. Liu, H. Li, L. Zhu, J. He, W. Jiang, W. Zhu and H. Li, *ACS Sustainable Chem. Eng.*, 2022, **10**, 4551–4560.
8 J.-R. Zhang, J. Yin, J. He, H.-S. Ran, W. Jiang, H.-P. Li, W.-S. Zhu, H.-M. Li and M. Zhang, *Pet. Sci.*, 2024, **21**, 2817–2829.
9 P. Wu, B. Wang, L. Chen, J. Zhu, N. Yang, L. Zhu, C. Deng, M. Hua, W. Zhu and C. Xu, *Adv. Sci.*, 2024, **11**, 2401996.
10 X. Zhou, T. Wang, D. He, P. Chen, H. Liu, H. Lv, H. Wu, D. Su, H. Pang and C. Wang, *Angew. Chem., Int. Ed.*, 2024, **63**, e202408989.
11 H. Lu, S. Wang, C. Deng, W. Ren and B. Guo, *J. Hazard. Mater.*, 2014, **279**, 220–225.
12 Y. Shiraishi and T. Hirai, *Energy Fuels*, 2004, **18**, 37–40.
13 X. Chen, S. Yuan, A. A. Abdeltawab, S. S. Al-Deyab, J. Zhang, L. Yu and G. Yu, *Sep. Purif. Technol.*, 2014, **133**, 187–193.
14 N. Jin, J. Yue, Y. Zhao, H. Lu and C. Wang, *Chem. Eng. J.*, 2021, **413**, 127419.
15 P. S. Kulkarni and C. A. M. Afonso, *Green Chem.*, 2010, **12**, 1139–1149.
16 C. Dai, J. Zhang, C. Huang and Z. Lei, *Chem. Rev.*, 2017, 6929–6983.
17 J. Wang, L. Zhang, Y. Sun, B. Jiang, Y. Chen, X. Gao and H. Yang, *Fuel Process. Technol.*, 2018, **177**, 81–88.
18 L. Zhang, J. Wang, Y. Sun, B. Jiang and H. Yang, *Chem. Eng. J.*, 2017, **328**, 445–453.
19 Y. Qiao, E. Shi, X. Wei and Z. Hou, *Green Chem.*, 2024, **26**, 5127–5149.
20 B. Wang, L. Qin, T. Mu, Z. Xue and G. Gao, *Chem. Rev.*, 2017, **117**, 7113–7131.
21 T. Zhang, T. Doert, H. Wang, S. Zhang and M. Ruck, *Angew. Chem., Int. Ed.*, 2021, **60**, 22148–22165.
22 A. A. Quintana, A. M. Sztapka, V. D. S. Ebinuma and C. Agatemor, *Angew. Chem., Int. Ed.*, 2022, **61**, e202205609.
23 Z. Jingyu, L. Shang, Y. Liping, Y. Yuexing, S. Lingqi, L. Zuguang and H. Qiu, *Chin. Chem. Lett.*, 2023, **34**, 107750.
24 Y.-X. Chen, M. Zhang, S.-Z. Zhang, Z.-Q. Hao and Z.-H. Zhang, *Green Chem.*, 2022, **24**, 4071–4081.
25 Y. Guan, Y.-L. Ying, B. Wang, L.-P. Mo and Z.-H. Zhang, *J. Catal.*, 2025, **443**, 107750.
26 E. Durand, J. Lecomte and P. Villeneuve, *Eur. J. Lipid Sci. Technol.*, 2013, **115**, 379–385.
27 J. Jiang, X. Bai, X. Zhao, W. Chen, T. Yu, Y. Li and T. Mu, *Green Chem.*, 2019, **21**, 5571–5578.
28 H. Qin, X. Hu, J. Wang, H. Cheng, L. Chen and Z. Qi, *Green Energy Environ.*, 2020, **5**, 8–21.
29 M. Zhang, X. Zhang, Y. Liu, K. Wu, Y. Zhu, H. Lu and B. Liang, *Environ. Sci. Pollut. Res.*, 2021, **28**, 35537–35563.
30 Z. Tong, J. Meng, S. Liu, Y. Liu, S. Zeng, L. Wang, Q. Xia and H. Yu, *Carbohydr. Polym.*, 2021, **272**, 118473.
31 Y. Luo, H. Ma, S. Zhang, D. Zheng, P. Che, X. Liu, M. Zhang, J. Gao and J. Xu, *J. Am. Chem. Soc.*, 2020, **142**, 6085–6092.
32 L. Sun, Z. Zhu, T. Su, W. Liao, D. Hao, Y. Chen, Y. Zhao, W. Ren, H. Ge and H. Lu, *Appl. Catal., B*, 2019, **255**, 117747.
33 L. Xu, J. Yin, J. He, L. Zhu, H. Ning, K. Jie, W. Zhu, H. Li, S. Dai and W. Jiang, *Adv. Mater.*, 2024, **36**, 231385.
34 W. Zhu, C. Wang, H. Li, P. Wu, S. Xun, W. Jiang, Z. Chen, Z. Zhao and H. Li, *Green Chem.*, 2015, **17**, 2464–2472.
35 B. Yang, K. Fan, S. Yu, X. Peng, T. Zhang, L. Zhang, F. Zhang, H. Wu, J. Guo and B. Liu, *J. Cleaner Prod.*, 2023, **406**, 136878.
36 D. Zhu, J. Yin, L. Xu, B. Zhang, L. Zhu, J. He, H. Li, W. Zhu, H. Li and W. Jiang, *Appl. Catal., B*, 2025, **363**, 124774.
37 I. Carson, M. R. Healy, E. D. Doidge, J. B. Love, C. A. Morrison and P. A. Tasker, *Coord. Chem. Rev.*, 2017, **335**, 150–171.

38 P. H. Mutin, G. Guerrero and A. Vioux, *C. R. Chim.*, 2003, **6**, 1153–1164.
39 M.-R. Liu, Y.-P. Lin, K. Wang, S. Chen, F. Wang and T. Zhou, *Chin. J. Catal.*, 2020, **41**, 1654–1662.
40 M. Kloda, S. Ondrusova, K. Lang and J. Demel, *Coord. Chem. Rev.*, 2021, **433**, 213748.
41 Y. Zuo, J. Wu, X. Chen, N. Wei and J. Tong, *Sep. Purif. Technol.*, 2023, **325**, 124714.
42 M. Chen, C. Zou, W. Tang and Y. Cao, *Sep. Purif. Technol.*, 2023, **323**, 124491.
43 X. He, Y. Wen, X. Wang, Y. Cui, L. Li and H. Ma, *Waste Manage.*, 2023, **157**, 8–16.
44 H. Wang, S. Liu, Y. Zhao, J. Wang and Z. Yu, *ACS Sustainable Chem. Eng.*, 2019, **7**, 7760–7767.
45 R. Saputra, R. Walvekar, M. Khalid and N. M. Mubarak, *J. Mol. Liq.*, 2020, **310**, 113232.
46 A. M. B. do Rego, A. M. Ferraria, J. El Beghdadi, F. Debontridder, P. Brogueira, R. Naaman and M. R. Vilar, *Langmuir*, 2005, **21**, 8765–8773.
47 T. Lu and F. Chen, *J. Comput. Chem.*, 2012, **33**, 580–592.
48 E. R. Johnson, S. Keinan, P. Mori-Sánchez, J. Contreras-García, A. J. Cohen and W. Yang, *J. Am. Chem. Soc.*, 2010, **132**, 6498–6506.
49 H. Yang, B. Jiang, Y. Sun, L. Hao, Z. Huang and L. Zhang, *Chem. Eng. J.*, 2016, **306**, 131–138.
50 F. Liu, J. Yu, A. B. Qazi, L. Zhang and X. Liu, *Environ. Sci. Technol.*, 2021, **55**, 1419–1435.
51 C.-F. Mao, R.-X. Zhao and X.-P. Li, *Fuel*, 2017, **189**, 400–407.
52 S. Guan, Z. Li, B. Xu, J. Wu, J. Han, T. Guan, J. Wang and K. Li, *ACS Sustainable Chem. Eng.*, 2023, **11**, 6292–6301.
53 S. Guan, Z. Li, B. Xu, J. Wu, N. Wang, J. Zhang, J. Han, T. Guan, J. Wang and K. Li, *Chem. Eng. J.*, 2022, **441**, 136022.
54 Z. Yu, X. Huang, S. Xun, M. He, L. Zhu, L. Wu, M. Yuan, W. Zhu and H. Li, *J. Mol. Liq.*, 2020, **308**, 113059.
55 W. Liang, S. Zhang, H. Li and G. Zhang, *Fuel Process. Technol.*, 2013, **109**, 27–31.
56 J. Zou, S. Wu, Y. Lin, X. Li, Q. Niu, S. He and C. Yang, *Environ. Sci. Technol.*, 2024, **58**, 14895–14905.
57 J. Guo, B. Li, D. Zhao, L. Chu, H. Yang, Z. Huang, Z. Liu, M. Yang and G. Wang, *Chem. Eng. J.*, 2023, **474**, 145853.
58 L. Chen, J.-T. Ren and Z.-Y. Yuan, *Chem. Eng. J.*, 2022, **450**, 138330.
59 J. Zou, X. Li, S. He, Q. Niu, S. Wu and C. Yang, *Adv. Funct. Mater.*, 2024, 2415558.
60 S. Zhou, Z. Wu, J. Liu, Y. Wang, S. Shao, F. Liu, H. Cheng, H. Liu, H. Li and W. Zhu, *Chem. Eng. J.*, 2024, **479**, 147776.
61 S. Shao, H. Liu, X. Wang, L. Jia, S. Zhou, Y. Huang, H. Cheng, F. Liu, Y. Wang, J. Liu and W. Zhu, *Chem. Eng. J.*, 2024, **495**, 153654.
62 W. Liu, T. Li, G. Yu, J. Wang, Z. Zhou and Z. Ren, *Fuel*, 2020, **265**, 116967.
63 L. Hao, M. Wang, W. Shan, C. Deng, W. Ren, Z. Shi and H. Lu, *J. Hazard. Mater.*, 2017, **339**, 216.
64 C.-F. Mao, R.-X. Zhao and X.-P. Li, *RSC Adv.*, 2017, **7**, 42590–42596.
65 D. Hao, L. Hao, C. Deng, W. Ren, C. Guo and H. Lu, *Chem. Eng. Technol.*, 2019, **42**, 1276–1282.
66 S. Guan, Z. Li, B. Xu, J. Wu, N. Wang, J. Zhang, J. Han, T. Guan, J. Wang and K. Li, *Chem. Eng. J.*, 2022, **441**, 136022.
67 Y. Guo, X. Liu, J. Li and B. Hu, *RSC Adv.*, 2021, **11**, 31727–31737.
68 W. Jiang, K. Zhu, H. Li, L. Zhu, M. Hua, J. Xiao, C. Wang, Z. Yang, G. Chen, W. Zhu, H. Li and S. Dai, *Chem. Eng. J.*, 2020, 124831.
69 C. Mao, R. Zhao, X. Li and X. Gao, *RSC Adv.*, 2017, **7**, 12805–12811.
70 B. Zhang, Z. Jiang, J. Li, Y. Zhang, F. Lin, Y. Liu and C. Li, *J. Catal.*, 2012, **287**, 5–12.
71 C. Li, D. Li, S. Zou, Z. Li, J. Yin, A. Wang, Y. Cui, Z. Yao and Q. Zhao, *Green Chem.*, 2013, **15**, 2793–2799.
72 S. Guan, Z. Li, B. Xu, J. Wu, J. Han, T. Guan, J. Wang and K. Li, *Fuel*, 2023, **333**, 126329.
73 H. Li, Y. Chang, W. Zhu, W. Jiang, M. Zhang, J. Xia, S. Yin and H. Li, *J. Phys. Chem. B*, 2015, **119**, 5995–6009.
74 S. Zahn, D. R. MacFarlane and E. I. Izgorodina, *Phys. Chem. Chem. Phys.*, 2013, **15**, 13664–13675.
75 T.-W. Kwon, Y. K. Jeong, I. Lee, T.-S. Kim, J. W. Choi and A. Coskun, *Adv. Mater.*, 2014, **26**, 7979–7985.
76 M. P. Waller and J. Yang, *Acta Crystallogr., Sect. A:Found. Crystallogr.*, 2013, **69**, S92–S92.

